AMERICAN SOCIETY FOR MICROBIOLOGY | Applied and Environmental Microbiology®

PHYSIOLOGY

Oxidation of Cytochrome 605 Is the Rate-Limiting Step when *Ferrimicrobium acidiphilum* Respires Aerobically on Soluble Iron

Robert C. Blake II,[a] Jessie J. Guidry,[b] Micah D. Anthony,[a]* Bhupal Ban,[a]* Kayla A. Smith,[a] Noelle N. Walton,[a] Richard G. Painter[a]*

[a]College of Pharmacy, Xavier University of Louisiana, New Orleans, Louisiana, USA
[b]LSUHSC Proteomics Core Facility, Louisiana State University Health Sciences Center, New Orleans, Louisiana, USA

ABSTRACT Proteins that oxidize extracellular substrates in Gram-positive bacteria are poorly understood. *Ferrimicrobium acidiphilum* is an actinobacterium that respires aerobically on extracellular ferrous ions at pH 1.5. *In situ* absorbance measurements were conducted on turbid suspensions of intact *Fm. acidiphilum* using an integrating cavity absorption meter designed for that purpose. Initial velocity kinetic studies monitored the appearance of product ferric ions in the presence of catalytic quantities of cells. Cell-catalyzed iron oxidation obeyed the Michaelis-Menten equation with K_m and V_{max} values of 71 μM and 0.29 fmol/min/cell, respectively. Limited-turnover kinetic studies were conducted with higher concentrations of cells to detect and monitor changes in the absorbance properties of cellular redox proteins when the cells were exposed to limited quantities of soluble reduced iron. A single *a*-type cytochrome with reduced absorbance peaks at 448 and 605 nm was the only redox-active chromophore that was visible as the cells respired aerobically on iron. The reduced cytochrome 605 exhibited mathematical and correlational properties that were consistent with the hypothesis that oxidation of the cytochrome constituted the rate-limiting step in the aerobic respiratory process, with a turnover number of 35 ± 2 s^{-1}. Genomic and proteomic analyses showed that *Fm. acidiphilum* could and did express only two *a*-type heme copper terminal oxidases. Cytochrome 605 was associated with the terminal oxidase gene that is located between nucleotides 31,090 and 33,039, inclusive, in the annotated circular genome of this bacterium.

IMPORTANCE The identities and functions of proteins involved in aerobic respiration on extracellular ferrous ions at acidic pH are poorly understood in the four phyla of Gram-positive eukaryotes and archaea where such activities occur. *In situ* absorbance measurements were conducted on *Fm. acidiphilum* as it respired on extracellular iron using an integrating cavity absorption meter that permitted accurate optical measurements in turbid suspensions of the intact bacterium under physiological conditions. The significance of these measurements is that they permitted a direct spectrophotometric examination of the extents and rates of biological electron transfer events *in situ* under noninvasive physiological conditions without disrupting the complexity of the live cellular environment. One thing is certain: one way to understand how a protein functions in an intact organism is to actually observe that protein as it functions in the intact organism. This paper provides an example of just such an observation.

KEYWORDS cytochrome oxidase, actinobacteria, respiratory chain, electron transfer, proteomics, systems biology, integrating cavity absorption meter, bioenergetics

Citation Blake RC, II, Guidry JJ, Anthony MD, Ban B, Smith KA, Walton NN, Painter RG. 2020. Oxidation of cytochrome 605 is the rate-limiting step when *Ferrimicrobium acidiphilum* respires aerobically on soluble iron. Appl Environ Microbiol 86:e01906-20. https://doi.org/10.1128/AEM.01906-20.

Editor Haruyuki Atomi, Kyoto University

Address correspondence to Robert C. Blake II, rblake@xula.edu.

* Present address: Micah D. Anthony, Bristol-Myers Squibb, Lawrenceville, NJ, USA; Bhupal Ban, Indiana Biosciences Research Institute, Indianapolis, IN, USA; Richard G. Painter, Metairie, LA, USA.

Received 3 August 2020
Accepted 3 September 2020
Accepted manuscript posted online 11 September 2020
Published 28 October 2020

Ferrimicrobium acidiphilum (*Fm. acidiphilum*) is a rod-shaped, mesophilic, obligately acidophilic eubacterium that was isolated from the waters of an abandoned sulfur mine in North Wales, UK (1). It is an obligately heterotrophic bacterium that also catalyzes the dissimilatory oxidation and reduction of soluble iron in the presence of organic carbon. Although it is a member of the Gram-positive *Actinobacteria* phylum, the organism itself stains Gram-negative. Other phenotypically similar bacteria in the same family (*Acidimicrobidae*) include *Acidimicrobium ferrooxidans* (2–4), *Ferrithrix thermotolerans* (1), and *Acidithrix ferrooxidans* (5). A fifth organism, *Acidithiomicrobium ferrooxidans*, has been reported that also oxidizes reduced sulfur (6, 7), but, unlike the other *Acidimicrobidae*, this last organism is not available from commercial culture collections.

Very little is known regarding the relevant electron transfer biomolecules expressed by those members of the *Actinobacteria* that conduct respiration on soluble iron. This laboratory conducted a survey of the cellular absorbance changes that occurred when soluble iron was mixed with intact cells of two different species derived from each of the 6 phyla that contain members that respire aerobically on iron (8). The survey instrument was a novel integrating cavity absorption meter (ICAM) that was designed to quantify the total measuring illumination that was introduced into an enclosed observation chamber. The premise was that suspensions of live bacteria within the observation chamber could be irradiated in an isotropic homogeneous field of incident measuring light, where the absorbed radiant power was expected to be independent of scattering effects (9–12). A total of 6 different patterns of iron-dependent absorbance changes were observed in these survey measurements (8). *Fm. acidiphilum* joined 3 other eubacteria derived from two Gram-positive phyla to yield iron-dependent absorbance changes that were attributed to changes in *a*-type hemeproteins that were hypothesized to represent parts of the terminal oxidases in their respective microorganisms.

The experiments presented below were undertaken to determine whether the appearance and disappearance of this *a*-type hemeprotein in *Fm. acidiphilum* could be correlated with the concomitant appearance of product ferric ions as the organism respired aerobically on soluble iron. The hypothesis was that the oxidation of this *a*-type hemeprotein, with its reduced peak at 605 nm, constituted the slowest, or rate-limiting, step when intact *Fm. acidiphilum* respired aerobically on reduced soluble iron. Relating the transient, iron-dependent absorbance changes in *Fm. acidiphilum* to the appearance of oxidized soluble iron is no different, in principle, than relating the transient absorbance changes in the colored prosthetic groups that are employed by purified oxidoreductases as they catalyze their individual reactions. Britton Chance demonstrated over 75 years ago that a 2-electron oxidized form of heme *b* was transiently formed when horseradish peroxidase was mixed with hydrogen peroxide (13). The resulting enzymatic Compound I fulfilled all of the mathematical and correlational requirements to represent the Michaelis complex in the horseradish peroxidase-catalyzed oxidation of malachite green by hydrogen peroxide. Chance's approach was later adapted to study the role of transient colored intermediates in flavoprotein oxidoreductases (14, and references therein). Others have substituted fluorescent analogs of substrates in the absence of colored prosthetic groups in the enzyme to visualize transient Michaelis complexes and investigate their roles in the overall catalytic cycles of the enzymes (15, 16). This paper exploits the same approach to study the role of transient absorbance changes in suspensions of intact *Fm. acidiphilum* as it respires aerobically on soluble iron. The transient spectral intermediate with a reduced peak at 605 nm is shown to fulfill all of the mathematical and correlational requirements to represent an obligatory intermediate in the respiratory electron transfer process catalyzed by the intact organism.

RESULTS

Cell culture. A principal datum in the interpretation of quantitative enzyme kinetic studies is the concentration and/or the amount of the enzyme catalyst. Similarly, a principal datum in the interpretation of quantitative kinetic studies as catalyzed by

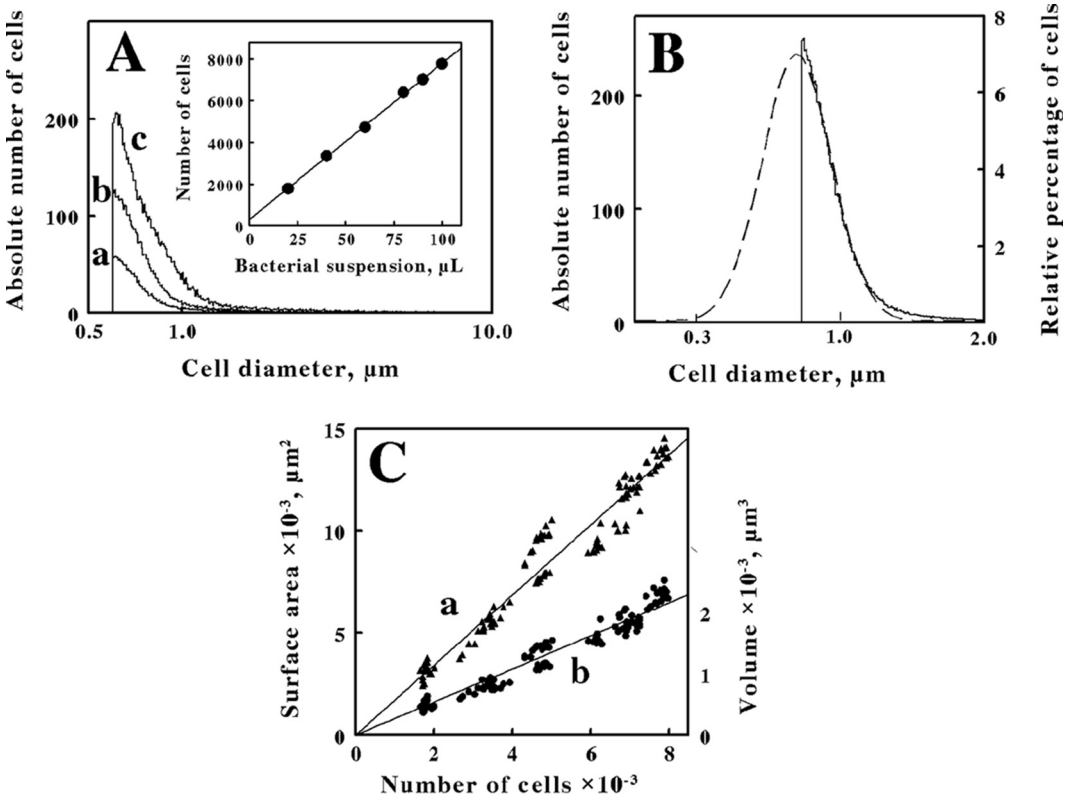

FIG 1 Quantification and characterization of intact *Fm. acidiphilum*. (A) Electrical impedance measurements of the absolute number of bacteria as a function of cell diameter. Curves *a*, *b*, and *c* represent 20, 60, and 100 μl, respectively, of a dilution of a stock suspension of bacteria. Inset, the number of cells as a function of the microliters of cell suspension. Each datum represents the mean of 20 determinations. (B) Comparison of cell suspensions by electrical impedance (solid curve, left ordinate) and static light diffraction (dashed curve, right ordinate) methods. The scale of each ordinate was chosen to facilitate comparison of the curves. The area under the electrical impedance curve was 47% of that under the light diffraction curve. (C) Dependences of the surface area (curve *a*, triangles) and volume (curve *b*, circles) of *Fm. acidiphilum* as a function of the number of cells. The lines drawn through the data points were determined by linear regression analyses.

intact cells is the number and/or the quantity of the cells themselves. Intact cells of *Fm. acidiphilum* were quantified by counting them as a function of their individual volumes by electrical impedance measurements in a Multisizer 4 particle counter. Figure 1A shows three representative examples of the number of cells as a function of cell size for different volumes of a diluted suspension of *Fm. acidiphilum*. Although the instrument actually measures the volume of each cell regardless of its shape, the instrumental software converts the different volumes to their mean spherical equivalents and displays the counts as a function of the diameters of these spherical equivalents. The inset of Fig. 1A shows the dependence of the number of cells on the volumes of a diluted cell suspension that were added to the electrolyte solution in the Multisizer. The number of cells was directly proportional to the volumes of cell suspension that were added to the electrolyte solution. These measurements provided the means to quantify the number of cells present in any stock suspension of cells that were used in subsequent kinetic measurements.

The solid curve in Fig. 1B shows the mean number of counts in each narrow size range for over 120 Multisizer assays of suspended *Fm. acidiphilum*. Bacteria with spherical equivalent diameters less than 0.6 μm were invisible in the electrical impedance measurements because the instrumental response was limited to particles with effective diameters between 2 and 60% of the 30-μm aperture employed in the instrument. It is evident from the shape of the solid curve in Fig. 1B that a number of smaller cells are invisible to this method. The dashed curve in Fig. 1B shows the relative numbers of *Fm. acidiphilum* cells as a function of spherical equivalent diameters as

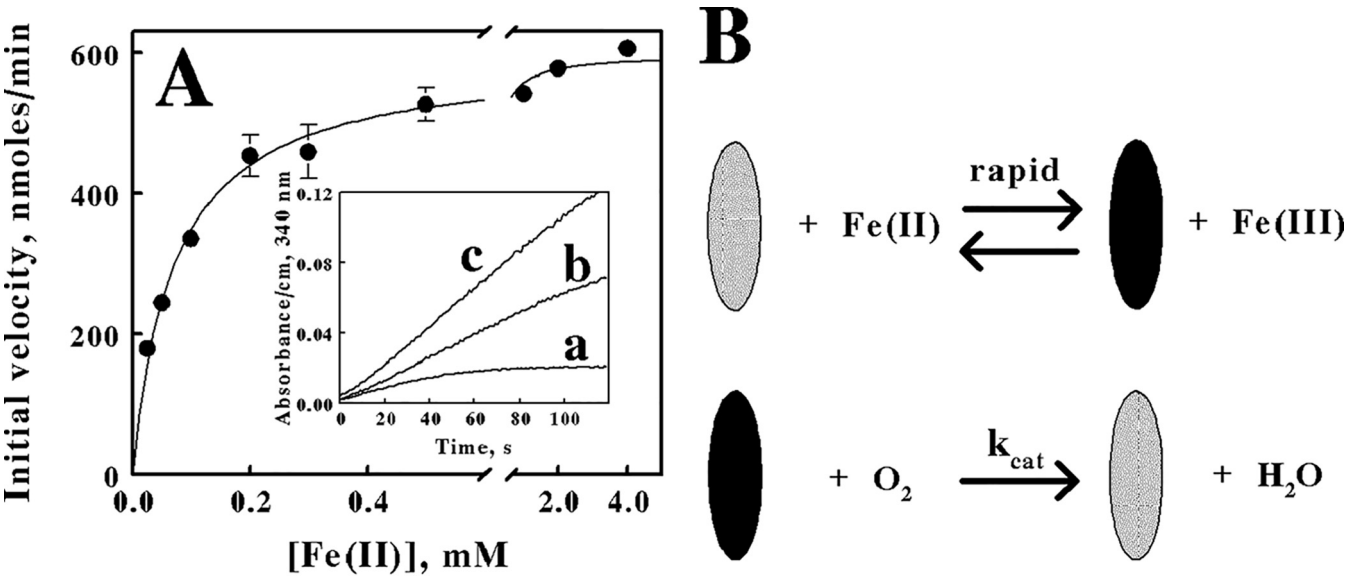

FIG 2 Kinetic behavior of aerobic respiration on soluble iron by *Fm. acidiphilum* conforms to the Michaelis-Menten equation. (A) Dependence of the initial velocity of ferric ion production on the concentration of ferrous ions when 2.0×10^9 cells of *Fm. acidiphilum* were included in 8 ml of sulfuric acid (pH 1.5) at 30°C. The parameters for the curve drawn through the data points were determined by a nonlinear regression analysis using the Michaelis-Menten equation. Inset, representative examples of the increases in absorbance at 340 nm as a function of time due to the bacterially catalyzed production of ferric ions. The initial concentrations of ferrous ions were 25, 100, and 1,000 μM in curves *a* to *c*, respectively. (B) Schematic representation of the kinetic mechanism for aerobic respiration on soluble iron as catalyzed by *Fm. acidiphilum*. The gray and black rods represent bacteria that contain oxidized and iron-reduced electron transport proteins, respectively.

determined by a laser light diffraction method. Light diffraction measurements are capable of resolving particles with effective diameters smaller than 0.1 μm. The electrical impedance and the light diffraction curves showed close correspondence down to 0.6 μm, indicating that the two instruments were monitoring the same population of particles. The area under the electrical impedance curve was 47% of that under the light diffraction curve. Consequently, the absolute counts of *Fm. acidiphilum* cells obtained by the electrical impedance method were multiplied by 2.13 to correct for the percentage of bacterial counts that were below the limit of detection of the instrument. Because slightly less than half of the cells were directly enumerated using the electrical impedance measurements, a value for the total cell protein was also independently determined to provide an alternative means to quantify the whole-cell catalyst. A wet cell paste that contained 10^{10} cells of *Fm. acidiphilum* yielded a mass of 360 μg of total protein. Thus, each cell was determined to contain 36 femtograms of protein.

Figure 1C shows the dependencies of the surface area and the volume of intact *Fm. acidiphilum* cells on the number of cells derived from over 120 assays using electrical impedance measurements. Each value of the volume represents the sum of the individual volumes for all of the cells measured in that particular assay. Each value of the surface area is the sum of individual surface areas calculated from the corresponding volumetric data assuming that each bacterial particle is a perfect sphere. *Fm. acidiphilum* is rod-shaped with an aspect ratio of ~1:4 (1). Consequently, the values of the surface areas calculated using the spherical model represent a conservative estimate of the true surface area; a more accurate estimate of the surface area of rounded rods with an average aspect ratio of 1:4 requires that the values of the surface areas in Fig. 1C be multiplied by a factor of 1.2. Average surface areas and volumes for intact *Fm. acidiphilum* cells of 1.71 ± 0.02 μm^2/cell and 0.27 ± 0.01 μm^3/cell, respectively, were obtained from the slopes of the two lines in Fig. 1C.

Initial velocity kinetic studies. Intact cells of *Fm. acidiphilum* began catalyzing the appearance of ferric ions as soon as they were introduced into an aerobic solution of ferrous ions in sulfuric acid, pH 1.5. The inset in Fig. 2A shows three representative time courses for the increases in absorbance at 340 nm that were obtained when 2.0×10^9

cells of *Fm. acidiphilum* were mixed with different concentrations of ferrous ions and monitored over time at 30°C. We determined an absorption coefficient of 890 $M^{-1}cm^{-1}$ at 340 nm for oxidized iron in sulfuric acid, pH 1.5 (see Fig. S1 in the supplemental material). Initial velocities of the changes in ferric concentration as a function of time were obtained from primary data such as those shown in the inset of Fig. 2A, and the resulting secondary plot of initial velocity as a function of the starting ferrous ion concentration is shown in the main panel. The parameters for the rectangular hyperbola drawn through the data points in Fig. 2A were derived from a nonlinear least-squares fit of the initial velocity data to the Michaelis-Menten equation. Values for K_m and V_{max} of $71 \pm 6\ \mu$M and 597 ± 10 nmol/min, respectively, were obtained from the analysis. That value of V_{max} corresponds to a turnover number of approximately 0.29 fmol/min/cell. It should be noted that the value of this turnover number is a minimal conservative estimate that depends upon the actual activity and viability of the intact cells in the denominator of this relationship. Aerobic respiration on soluble iron could not be detected by absorbance measurements at 340 nm when *Fm. acidiphilum* was heat-inactivated by incubating a suspension at 90°C for 30 min. If, however, a percentage of the intact cells had a lower activity than that of the others, the value of the actual maximum turnover number would necessarily be a larger number. Nonetheless, it is reassuring that the value calculated here is consistent with the results of the subsequent activity measurements with higher concentrations of cells, which are presented and described below.

The schematic illustration shown in Fig. 2B represents the minimal kinetic mechanism that is consistent with the initial velocity kinetic data shown in Fig. 2A. The iron-dependent reduction of any relevant electron transport proteins in the bacterium is shown as a relatively rapid reaction, which is consistent with observations that reduction of a component within the intact cell is complete within the 0.5 s dead time of the mixing, even when the concentration of ferrous ions is only 50 μM (see below). The bacterium with its reduced cellular component(s) then reacts with molecular oxygen to regenerate the oxidized bacterium in a slower reaction that constitutes the rate-limiting catalytic step. Because *Fm. acidiphilum* is known to both oxidize and reduce soluble iron (1), the exchange of electrons between the bacterium and soluble iron is depicted in Fig. 2B as a reversible reaction. When the concentration of intact *Fm. acidiphilum* cells is limited to that of a catalyst compared with the concentrations of reduced iron and molecular oxygen, aerobic respiration on soluble iron proceeds kinetically in a manner that is consistent with the Michaelis-Menten formalism.

Reduction of the bacterium. Preliminary survey studies have shown that intact *Fm. acidiphilum* exhibits changes in its absorbance spectrum when it is exposed to soluble ferrous ions (8). The dashed curve in Fig. 3 shows the visible absorbance spectrum of air-oxidized *Fm. acidiphilum* that was obtained in the CLARiTY spectrophotometer in sulfuric acid, pH 1.5. Even though the cell suspension contained 1.1×10^{10} cells in 8 ml and was very turbid, the absorbance spectrum of the oxidized organism contained no trace of the light-scattering artifacts that one would observe by conducting the same absorbance measurements using a conventional linear spectrophotometer. The oxidized spectrum in Fig. 3 showed a clearly defined Soret peak at 418 nm.

The solid curve in Fig. 3 shows the absorbance spectrum that was obtained after 0.5 s when the cells of *Fm. acidiphilum* were exposed to 4.0 mM ferrous ions. Exposure to soluble reduced iron caused the Soret peak to decrease somewhat in amplitude and assume an evident shoulder at around 445 nm. In addition, a prominent peak appeared in the reduced absorbance spectrum at 605 nm. Even though the intact organism was conducting aerobic respiration on the soluble iron during these measurements, the concentration of ferrous ions (4.0 mM) sufficiently exceeded that of molecular oxygen ($\sim$240 μM) so as to ensure that the iron-reduced spectrum would persist long enough to conduct an accurate, semistable absorbance measurement of the iron-reduced form. Indeed, the reduced spectrum was unchanged for the entire 2 min of the observation; complete depletion of the dissolved O_2 would only consume approximately one

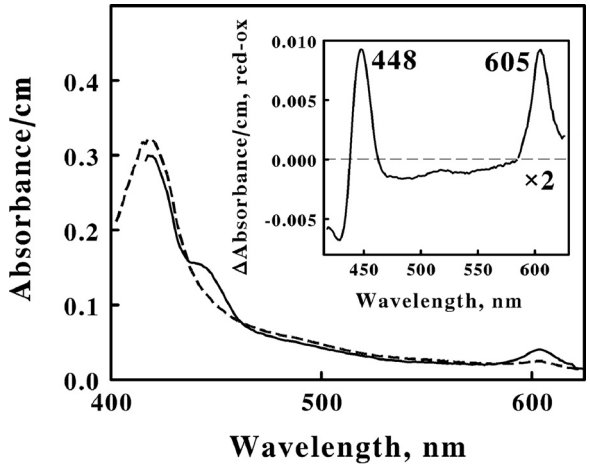

FIG 3 Identification of the principal electron transfer component that was reduced when *Fm. acidiphilum* was exposed to soluble iron. Absorbance spectra taken before (dashed curve) and 0.5 s after (solid curve) *Fm. acidiphilum* was mixed with 4.0 mM ferrous sulfate (pH 1.5) at 30°C. The final bacterial suspension contained 5.1×10^{10} cells in 8 ml. Inset, difference spectrum representing the absolute spectrum of the iron-reduced bacterium minus that of the air-oxidized bacterium.

quarter of the electrons available from the 4.0 mM Fe(II). The inset of Fig. 3 shows a reduced minus oxidized difference spectrum derived from the absorbance spectra shown in the main panel. The peaks observed in the difference spectrum at 448 and 605 nm are those that are frequently associated with cytochromes that contain *a*-type hemes (17). The extraordinary signal-to-noise characteristics of the small absorbance changes represented by the difference spectrum can be attributed to two factors. First, the difference spectrum itself was the average of 744 scans (120 s $\times$ 6.2 scans/s). Second, the many transversals through and within the observation chamber that the average photon must undergo to eventually exit the observation cell of an integrating cavity absorption meter dictates that the effective path length in a spherical, 8-ml chamber is roughly 15 cm (data not shown).

Prior absorbance measurements conducted on iron-reduced intact *Acidithiobacillus ferrooxidans* benefited from the fact that the absorption coefficients of that organism's principal respiratory components were available from multiple studies on the individual purified proteins (18–23). Thus, the average content of each iron-responsive electron transport protein could be calculated on a per-cell basis from absorbance measurements on intact cells (24). Terminal *a*-type heme copper oxidases have not been purified and characterized from cell extracts of *Fm. acidiphilum* or any of its phylogenetically close, iron-oxidizing relatives. Nonetheless, interesting estimations are possible using data extracted from the inset of Fig. 3. The typical mammalian heme copper terminal oxidase has a reduced *alpha* absorbance peak at 605 nm. Over 50 years ago, van Gelder reported a reduced minus oxidized absorption coefficient at 605 nm for the *a*-type hemes of the mammalian oxidase of 24 $mM^{-1}cm^{-1}$ (25). That value was actually comprised of unequal contributions from the *a*- and a_3-type hemes in the oxidase, but it nevertheless represents the absorption coefficient at 605 nm for that type of terminal oxidase. When that absorption coefficient is applied to the change in absorbance at 605 nm of 0.0046 taken from the inset of Fig. 3, then the 8 ml of the observation cavity is estimated to have contained 1.54 nmol or 9.25×10^{14} molecules of the *a*-type terminal oxidase. Each bacterial cell may then be calculated to contain an average of 8.4×10^4 hemes that absorb at 605 nm in the reduced state because the observation cavity contained 1.1×10^{10} intact cells. Finally, (i) the terminal oxidase is likely to be embedded in the plasma membrane and (ii) each cell has an average outer surface area of 1.71 μm^2 (see Fig. 1C). Consequently, a cytochrome 605 may be found, on the average, within every 20.7 nm^2 on the surface of the organism's plasma membrane. This calculation is a conservative estimate that is based on the minimum surface area

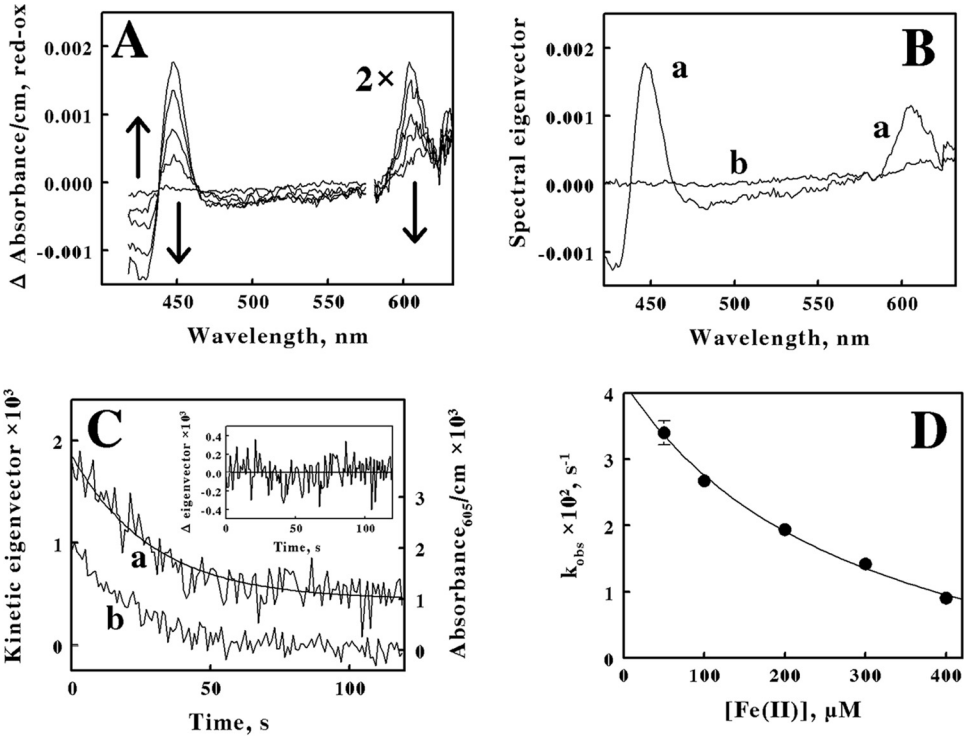

FIG 4 Oxidation kinetics of iron-reduced *Fm. acidiphilum*. (A) Difference spectra representing the absolute spectra of iron-reduced cells minus that of iron-oxidized cells at selected time intervals after 5.1×10^{10} cells of *Fm. acidiphilum* were mixed with 50 μM ferrous sulfate, pH 1.5. The reaction was monitored at 30°C in a dual-beam CLARiTY spectrophotometer equipped with a rapid-scan module. Six scans from 417 to 631 nm were taken every second for 120 s; spectra representing an average of 6 scans each and recorded at time delays of 1, 10, 20, 40, and 120 s after the addition of Fe(II) are presented. Each arrow indicates whether the apparent absorbance at that wavelength increased or decreased with time. (B) Spectral eigenvectors of the principal light-absorbing species present in the intact bacteria. Spectra were computed from a global fit of the data set represented in (A) to a single exponential function of time assuming the existence of two major species. Difference spectrum *a* was identical to that obtained 0.5 s after the cells were mixed with ferrous ions; difference spectrum *b* was identical to that obtained after the time-dependent absorbance changes were complete. (C) Comparison of the time-dependent oxidation of the bacteria monitored at 605 nm (*b*) with the kinetic eigenvector obtained from the global fit kinetic analysis (*a*). The smooth curve drawn through the *a* data represents a single exponential function of time with an apparent first order rate constant of 0.034 s^{-1}. Inset, a residual plot of the differences between the kinetic eigenvector and the computed single exponential function of time. (D) Dependence of the observed rate constants for the air oxidation of reduced *Fm. acidiphilum* on the initial concentration of ferrous iron. Each datum represents the mean and standard deviation of at least four determinations.

that is presented by a spherical shell. *Fm. acidiphilum* has a thick cell wall, as do all members of the *Actinobacteria*, and no notable convolutions of the confined plasma membrane have been reported in this or closely related organisms.

Oxidation of the bacterium. Under solution conditions where the initial concentrations of ferrous ions were less than or equal to 400 μM, the absorbance spectra of the cell suspensions that were exposed to soluble iron gradually changed from their partially reduced forms back to their original air-oxidized form as the aerobic respiration on the limiting iron electron donor proceeded to effective completion. Figure 4A shows a series of rapid kinetic scans obtained when a cell suspension was mixed with 50 μM ferrous sulfate at pH 1.5. The data comprise corrected difference spectra representing the absolute absorbance spectra of the iron-reduced *Fm. acidiphilum* obtained at various time points following the rapid reduction of the bacteria. The two prominent peaks of the difference spectra occur at 448 and 605 nm; there is a broad, shallow trough of lower absorbance between the two peaks. The observation of at least two well-defined isosbestic points at 438 and 460 nm, as well as two probable, additional isosbestic points at 588 and 620 nm, is extraordinary, considering that the spectra were acquired in a highly turbid suspension of intact bacteria. An isosbestic

point is a specific wavelength at which two or more absorbing species have the same molar absorptivity. The existence of these isosbestic points suggests that there is only one principal iron-responsive cytochrome that is visible in the respiratory chain of *Fm. acidiphilum* as it respires aerobically on soluble iron. It is useful at this point to recall that direct observations of electron transfer reactions in intact bacteria are subject to the same limitations as are those imposed upon any spectrophotometric observations. There are at least 4 principal reasons why other electron transfer-dependent absorbance changes were not detected in the absorbance measurements described herein: (i) the other colored biological agents were not transiently reduced or oxidized by electrons derived from extracellular iron; (ii) the other colored biomolecules had considerably smaller absorption coefficients; (iii) the other colored biomolecules were present at considerably lower concentrations; and (iv) the kinetic properties of the reduction and oxidation of other colored biomolecules were such that their accompanying transient absorbance changes could not be readily detected in our measurements.

After the initial rapid, iron-dependent reduction of the cytochrome 605 in the bacteria, the absorbance of the intact bacterium gradually returned to that observed originally in the air-oxidized state. Figure 4B shows the spectral eigenvectors that were calculated from a multiwavelength global fit of the data set in Fig. 4A to a single exponential function of time (*t*) as shown in equation 1,

$$\text{Absorbance} = (a - b)\, e^{-kt} + b \quad (1)$$

where *a* represents the spectrum of the reduced form of the bacterial suspension that was observed 0.5 s after mixing the cells with the soluble iron, *b* represents the spectrum of the final oxidized form of the suspension present at the end of the reaction, and *k* is the single pseudo first-order rate constant for all of the absorbance changes.

The kinetic eigenvector obtained from the global fit analysis is represented by curve *a* in Fig. 4C. The smooth curve in Fig. 4C drawn through the eigenvector data represents a single exponential function of time with a rate constant of 0.034 s^{-1}. Curve *b* in Fig. 4C shows the actual absorbance changes at 605 nm that were extracted from the data set in Fig. 4A. The close correspondence between the actual absorbance at 448 nm and the computed eigenvector absorbances is evident. Favorable comparisons such as that shown in Fig. 4C were also obtained with data extracted at 448 nm (data not shown).

Data sets analogous to that shown in Fig. 4A were also generated when intact *Fm. acidiphilum* cells were mixed with different concentrations of ferrous sulfate. Regardless of the starting concentration of ferrous sulfate, the resulting body of multiwavelength absorbance changes could be adequately described by a single exponential function of time. Figure 4D shows the dependence of the pseudo first-order rate constants obtained from these global fit analyses on the concentration of ferrous ions. As the initial concentrations of reduced iron increased, the observed rates of oxidation of the reduced form of cellular cytochrome 605 back to its original oxidized state decreased.

Cell-monitored turnover studies. The goal of these cell-monitored turnover studies was to examine the relationship, if any, between the cytochrome 605 that was reduced when intact cells were exposed to soluble ferrous ions and the rate and extent of the appearance of product ferric ions as the organism respired aerobically on reduced iron. The hypothesis was that oxidation of this reduced cytochrome constituted the rate-limiting step in this particular respiratory process. Any kinetic mechanism that conforms to the Michaelis-Menten formalism as illustrated schematically in Fig. 2B predicts that the velocity of product formation must be directly proportional to the concentration of the catalyst-substrate complex from which product formation occurs in the rate-limiting step. In this context, the catalyst-substrate complex is represented by the intracellular reduced cytochrome 605. The close correspondence between the time-dependent appearance of ferric ions and the concomitant disappearance of reduced cytochrome 605 is illustrated with the two kinetic traces shown in Fig. 5A. Curve *a* shows the increase in absorbance at 340 nm that signified the appearance of

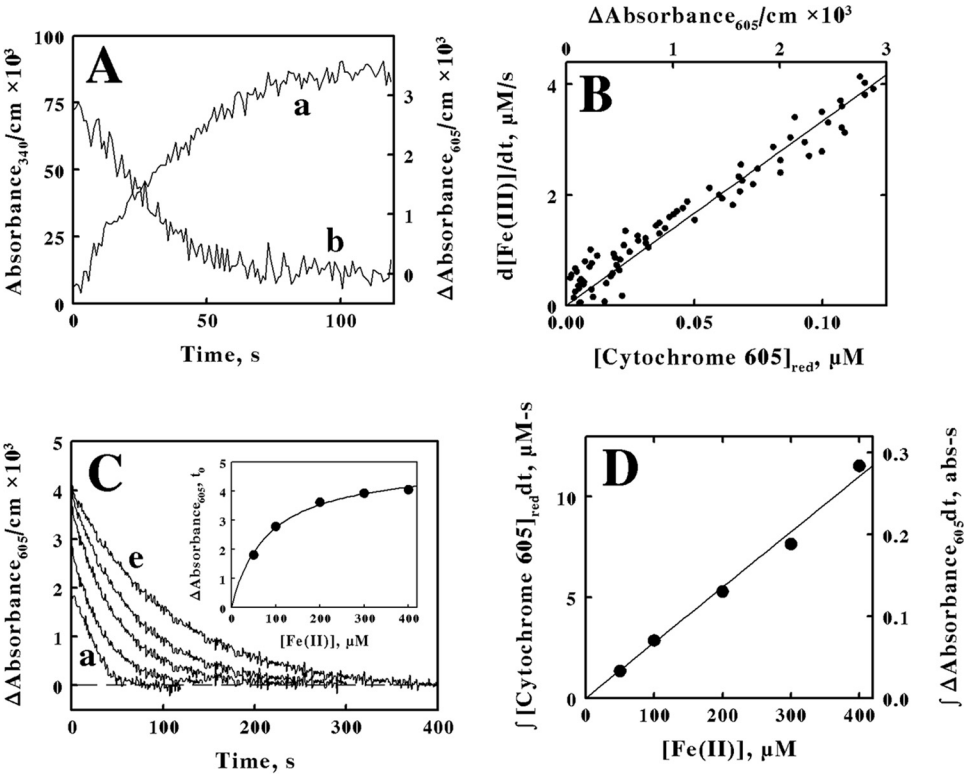

FIG 5 Absorbance of the reduced cytochrome 605 in intact *Fm. acidiphilum* correlates with the production of ferric ions during aerobic respiration on soluble iron. (A) Time courses of the changes in absorbance at 340 (*a*) and 605 (*b*) nm obtained when 5.1×10^{10} cells of *Fm. aciphilum* were mixed with 100 μM ferrous sulfate, pH 1.5. (B) Dependence of the velocity of ferric ion formation on the difference in absorbance values at 605 nm (upper abscissa) or the corresponding concentrations of reduced cytochrome 605 (lower abscissa). (C) Time courses of the changes in absorbance at 605 nm obtained when 5.1×10^{10} cells were mixed with 50, 100, 200, 300, and 400 μM ferrous sulfate in curves *a* to *e*, respectively. Inset, dependence of the absorbance differences observed 0.5 s after mixing on the starting concentration of ferrous iron. The parameters for the hyperbolic curve drawn through the data points were determined by nonlinear regression analysis. (D) Dependence of the integral over time of the absorbance change at 605 nm (right ordinate) or the concentration of reduced cytochrome 605 (left ordinate) on the concentration of total ferrous ions.

product ferric ions. Curve *b* shows the decrease in absorbance at 605 nm that signified the conversion of reduced cytochrome 605 back to its oxidized state. This increase at 340 nm is judged to be primarily due to the appearance of product ferric ions because (i) the total magnitude of the absorbance change at 340 nm is 25-fold greater than that at 605 nm (Fig. 5A) and (ii) cytochrome oxidase exhibits a negligible change in its absorbance properties at 340 nm (26). Both curves in Fig. 5A could be described mathematically as single exponential functions of time. The pseudo first-order rate constants for the increase in absorbance at 340 nm and the decrease in absorbance at 605 nm were 0.025 and 0.027 s^{-1}, respectively.

Figure 5B shows the initial rate of ferric formation as a function of the concentration of the reduced intracellular cytochrome 605. Values on the ordinate axis were obtained by (i) evaluating the time derivative of the exponential function that described curve *a* in Fig. 5A and then (ii) converting the absorbance values at 340 nm into their corresponding ferric ion concentrations. Corresponding values on the abscissa were obtained by (i) plotting the appropriate values of the Δabsorbance that remained at 605 nm (upper *x* axis) and then (ii) converting those $\Delta\text{absorbance}_{605}$ values to actual concentrations of the reduced cytochrome 605 using the absorption coefficient of 24 $mM^{-1}cm^{-1}$ (lower *x* axis). The data in Fig. 5B are consistent with equation 2:

$$\mathrm{d}\left[\mathrm{Fe(III)}\right]/\mathrm{dt} = k_{\mathrm{cat}}\left[\text{cytochrome 605}\right]_{\mathrm{red}} \quad (2)$$

where k_{cat} represents the turnover number if the oxidation of reduced cytochrome 605

is the rate-limiting step when *Fm. acidiphilum* respires aerobically on reduced iron. The slope of the linear regression line drawn through the data points in Fig. 5B was 33 s^{-1}, which represents the value of the rate-limiting k_{cat}. This value for k_{cat} is comparable to that calculated from the initial velocity kinetic studies presented above. Figure 2A produced a turnover number of 0.29 fmol/min/cell. If one converts (i) the minutes to seconds and (ii) the cell to moles of cells using Avogadro's number and then (iii) substitutes 8.4×10^4 cytochromes 605 per cell (see above), the turnover extracted from the initial velocity data is 35 s^{-1}.

Another prediction that is generated from the Michaelis-Menten formalism is that the total amount of product formed (or substrate consumed) must be directly proportional to the integral over time of the concentration of the limiting catalyst complex:

$$\left[\mathrm{Fe(III)}\right]_{\mathrm{formed}} = \left[\mathrm{Fe(II)}\right]_{\mathrm{consumed}} = k_{\mathrm{cat}} \int \left[\mathrm{cytochrome\ 605}\right]_{\mathrm{red}} \mathrm{dt} \quad (3)$$

Figure 5C shows a series of time-dependent oxidations of reduced cytochrome 605 after the intact organism was mixed with different concentrations of ferrous ions. These data are examples of those used to calculate the observed oxidation rate constants shown in Fig. 4D. The inset in Fig. 5C shows the dependence of the initial increases in the absorbance at 605 nm that were observed within 0.5 s upon mixing with ferrous ions on the concentration of the reduced iron. The data in the inset were fit to a rectangular hyperbola with a half-maximal concentration value of 81 μM, similar to the K_m value of 71 μM extracted from the initial velocity data shown in Fig. 2A.

The area beneath each oxidation curve in Fig. 5C represent the integrals over time swept out by the absorbance at 605 nm as the reduced cytochrome 605 returned to its original air-oxidized resting state. The right ordinate in Fig. 5D shows the dependence of the integral over time of the absorbance at 605 nm as a function of the starting concentration of ferrous ions. The left ordinate in Fig. 5D shows the dependence on starting iron concentrations after the absorbance at 605 nm was converted to the concentration of reduced cytochrome 605. The slope of the linear regression line drawn through the data points in Fig. 5D was 0.0275 s; the reciprocal of that slope, 36 s^{-1}, represents the third value for the k_{cat} that was extracted from these studies. The three values for k_{cat} obtained from different measurements are comparable, which provides evidence that is consistent with the hypothesis that the oxidation of reduced cytochrome 605 is indeed the rate-limiting step when *Fm. acidiphilum* respires aerobically on reduced iron.

Terminal oxidases in *Fm. acidiphilum*. The spectral properties featured in the inset of Fig. 3 are those typically associated with *a*-type hemes present in heme copper terminal oxidases in other organisms. Therefore, it was of interest to catalogue the types of terminal oxidases that could be expressed by *Fm. acidiphilum*. The genomic sequence of *Fm. acidiphilum* is published (27) and is available for appropriate searching activities in the RefSeq genome database. tBLASTn searches were conducted on the genomic sequence of *Fm. acidiphilum* using query sequences derived from each of the five heme copper oxidases that are generally recognized to comprise distinct, but nonetheless related, types of terminal oxidases (28, 29). Similar searches were also conducted for protein sequences associated with the *bd*-type terminal oxidases, a separate family of terminal oxidases that are clearly distinct from those within the larger family of heme copper oxidases (30, 31). These searches revealed that *Fm. acidiphilum* contained the sequence information to express only two different heme copper terminal oxidases.

The multimeric oxidase encoded by the gene cluster between bases 30,159 and 33,698 in the circular bacterial genome is represented schematically by the solid arrows in Fig. 6A. The contents of this cluster predict an oxidase comprised of three subunits whose amino acid sequences most closely resemble those of a classic aa_3-type of heme copper oxidase. The oxidase encoded by the gene cluster between bases 127,819 and 134,691 is represented schematically by the solid arrows in Fig. 6B. The terminal oxidase genes in this cluster also predict an oxidase that closely resembles an aa_3-type of oxidase. The latter gene cluster also includes the sequences to express the three protein

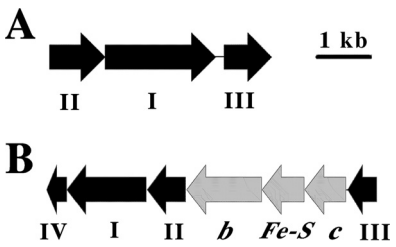

FIG 6 Order of the genes in the two gene clusters that encode proteins that comprise heme copper terminal oxidases in *Fm. acidiphilum*. (A) Locus tags FEAC_RS11730 to _RS11740, inclusive. (B) Locus tags FEAC_RS03375 to _RS03405, inclusive. The black arrows represent subunits of heme copper oxidases while the Roman numerals identify the type of subunit. The gray arrows represent the subunits of a quinol oxidase where *b*, *Fe-S*, and *c* identify subunits that contain cytochrome *b*, iron-sulfur groups, and cytochrome *c*, respectively.

components to comprise a typical bacterial quinol-*cytochrome c* oxidoreductase. Given that *Fm. acidiphilum* can grow both chemolithotrophically (on high reduction potential iron) and heterotrophically (on selected low reduction potential carbon compounds) (1), it is tempting to hypothesize that the oxidase represented by Fig. 6A is expressed during chemolithotrophic growth on substrates of high reduction potential like soluble iron, while the complex III/IV-types of combined oxidases represented in Fig. 6B are expressed during heterotrophic growth on carbon substrates of lower reduction potential.

Proteomic analyses were then conducted on cell extracts of *Fm. acidiphilum* that had been cultured mixotrophically on ferrous ions plus small amounts of yeast extract. The purpose of these analyses was to test the hypothesis posed in the previous paragraph, that the oxidase proteins represented in Fig. 6A should outnumber the oxidase proteins represented in Fig. 6B when the cells were cultured predominantly on soluble iron. The results of these analyses are summarized in Fig. 7. The three solid bars in Fig. 7 represent the quantities of distinct peptides derived from the three proteins that comprise the heme copper terminal oxidase in Fig. 6A. The three crosshatched bars in Fig. 7 represent the quantities of distinct peptides derived from the three proteins that comprise the heme copper terminal oxidase in Fig. 6B. It is generally acknowledged that this particular type of proteomic analysis is not strictly quantitative. Nonetheless, the sum of the peptide spectrum matches in the three solid bars is 1,943, while the corresponding sum in the three crosshatched bars is only 409, only a little over 20% of that of the higher total. This comparison provides evidence that is consistent with the hypothesis that cytochrome 605 is likely to be the same protein as that represented by protein accession number WP_052566320.1.

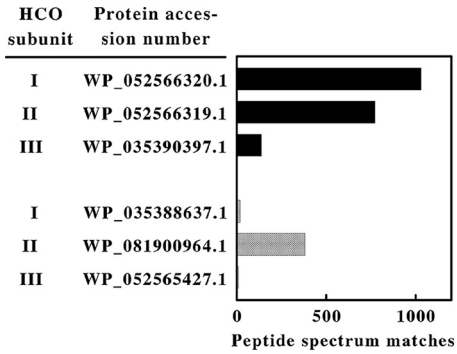

FIG 7 Proteomic analyses showing the relative yields of the individual subunits that comprise each of the two terminal oxidases encoded in the genome of *Fm. acidiphilum*. The first column represents the identities of the subunits of the two heme copper oxidases (HCO). The solid bars represent the subunits encoded by the locus tags FEAC_RS11730 to _RS11740, inclusive. The crosshatched bars represent the subunits encoded by the locus tags FEAC_RS03375 to _RS03385, inclusive.

DISCUSSION

It is generally acknowledged that iron ions do not enter the neutrophilic cytoplasm of those microorganisms that conduct dissimilatory oxidation of soluble iron to achieve the bulk of their energy needs. Rather, electrons derived from the oxidation of extracellular iron are transported by cellular biomolecules to a terminal oxidase that spans the plasma membrane. Prior detailed *in situ* spectroscopic studies have examined three species of Gram-negative eubacteria that respire aerobically on reduced iron (24, 32, 33). Gram-negative bacteria are likely to possess a minimum of three different electron transfer proteins to conduct electrons from their exterior to the interior of the cell: (i) an initial electron acceptor (and iron oxidase) in the outer membrane; (ii) a transient carrier to transport those electrons across the periplasm; and (iii) a terminal oxidase in the plasma membrane that catalyzes the reduction of molecular oxygen, presumably on the cytoplasmic side of the plasma membrane. In the case of *Acidithiobacillus ferrooxidans*, all three electron transfer components were visible *in situ*, and the entire multicenter ensemble behaved as would a single protein with a single macroscopic oxidation rate constant and a shared standard reduction potential of 650 mV (24). In the cases of both *Leptospirillum ferrooxidans* and *L. ferriphilum*, only a single respiratory protein was observed during *in situ* observations of aerobic respiration on soluble iron (32, 33). The protein, a cytochrome with a novel reduced peak at 579 nm, is presumed to serve as the periplasmic electron shuttle from a cytochrome 572 located in the organism's outer membrane (34) to the terminal oxidase (35), either a cbb_3-type of heme copper oxidase or a *bd*-type of terminal oxidase, in the plasma membrane. One hypothesis that is consistent with these latter *in situ* studies is that the oxidation of reduced cytochrome 579 constitutes the rate-limiting step in the aerobic iron respiratory chains of both organisms (32, 33).

Fm. acidiphilum is the first microorganism from a Gram-positive phylum that has been subjected to a detailed *in situ* spectroscopic study while it is respiring aerobically on soluble iron. As was the case with the two *Leptospirillum* species, only a single respiratory protein was visible when *Fm. acidiphilum* conducted aerobic respiration on limited concentrations of iron. In contrast to the two *Leptospirillum* species, where oxidation of a putative periplasmic electron carrier that is upstream from the terminal oxidase appeared to be the rate-limiting step (31, 32) in those Gram-negative respiratory chains, oxidation of the likely terminal oxidase itself appeared to be the rate-limiting step in the corresponding *Fm. acidiphilum*-catalyzed aerobic iron oxidation. It is notable that *Fm. acidiphilum* joined three other eubacteria derived from two Gram-positive phyla, together with two archaea from the *Euryarchaeota* phylum, to yield iron-dependent absorbance changes that were attributed to changes in *a*-type heme-proteins hypothesized to represent parts of the terminal oxidases in their respective microorganisms (8, 33). Perhaps rate-limiting oxidation of the terminal oxidase is the rule rather than the exception when dealing with chemolithotrophic microorganisms that respire aerobically on soluble iron.

The obvious structural differences among these organisms are that members of the *Actinobacteria* phylum do not have outer membranes, nor do they have periplasms. Consequently, soluble ferrous ions must penetrate the presumably thick outer cell wall of the organism to deposit their electrons with biomolecules on or within the organism's plasma membrane. The peptidoglycans that comprise at least 90% of the thick cell wall that surrounds this type of bacterium are porous to water and solutes with molecular masses less than approximately 1,000 Da (36). Others have shown that the diffusivity of sucrose in the peptidoglycan-like cell walls of selected plant cells is 15% to 20% of its value in water (37). Consequently, it is reasonable to hypothesize that soluble iron can diffuse, albeit more slowly than it can in water, among the interstitial spaces within the bacterium's cell wall to the surface of the plasma membrane. Alternatively, a network of iron atoms transiently trapped within the negatively charged cell wall could serve as an impromptu conduit to pass electrons from a ferrous ion near the outer surface of the cell wall to the plasma membrane on the inner side. The cell

walls of Gram-positive bacteria contain large quantities of teichoic and lipoteichoic phosphodiesters, as well as mono-attached teichoic acids (38). The pKa values of the former are 3.2 to 3.5, while the pKa values of the latter are 0.2 to 2.91 (39). Even a protonated phosphodiester or a mono-attached teichoic acid will simply exhibit a lower affinity for soluble iron than would the corresponding negatively charged conjugate base. Thus, there are ample opportunities to retain a network of soluble iron within the generally porous cell wall to serve as a conduit for electrons from the extracellular milieu to the plasma membrane. Whatever the detailed mechanism, it is prudent to remember that the iron-dependent reduction of cellular cytochrome 605 was complete within the practical dead time of approximately 0.5 s observed in our *in situ* measurements.

If there are no outer membrane and periplasm to cross, how many protein-protein electron transfer events are necessary until the electrons reach the terminal oxidase, where they are combined with molecular oxygen to create water? Recall that there is very little thermodynamic free energy available to those bacteria that conduct aerobic respiration on soluble iron. The reduction potential of soluble iron in sulfate media below pH 2.0 is between 650 and 750 mV versus the standard hydrogen electrode, depending on the concentration of sulfate ion (19). The corresponding reduction potential for the oxygen/water couple is 1120 mV at pH 2.0 (40). That means that around 350 mV, or 8.1 kcal/mol, are available from aerobic respiration to drive ATP synthesis by the Mitchell hypothesis. It has been argued that at least two ferrous ions must be oxidized to provide sufficient redox energy to phosphorylate one ADP to ATP (41, 42). Regardless of whether one, two, or even more ferrous ions must be oxidized to provide sufficient energy to generate each ATP, it is evident that the iron to molecular oxygen portion of the relevant electron transport chain must be relatively short, so as to not lose or waste energy as heat during multiple electron transfer steps. If cytochrome 605 represents the terminal oxidase in the aerobic iron respiratory chain of *Fm. acidiphilum*, what prevents the same protein complex from also serving as the iron oxidase, the initial electron acceptor from ferrous ions on the outer face of the plasma membrane? There were no other obvious electron transfer proteins encoded in the genome in the vicinity of the gene cluster associated with the loci that comprised the terminal oxidase that likely included cytochrome 605, the loci FEAC_RS11730 to FEAC_RS11740, inclusive. There is perhaps no need to posit an additional electron carrier between soluble ferrous ions and the terminal oxidase, one that could serve as a switching point for electrons destined either for energy generation or for the "uphill" transfer of electrons to generate NAD(P)H. The generation of suitable biochemical reducing equivalents is always an issue in those chemolithotrophs that oxidize substrates of high reduction potential like ferrous ions. In this case, there is no evidence that *Fm. acidiphilum* must conduct the energetically unfavorable transfer of electrons from a donor at 650 mV to an acceptor at −320 mV. Rather, it is entirely possible that *Fm. acidiphilum* can fulfill its requirements for biochemical reducing equivalents from the heterotrophic portion of its catabolic metabolism.

MATERIALS AND METHODS

Cell culture. *Ferrimicrobium acidiphilum* strain DSMZ 19497^T was cultured on the mixotrophic medium (20 mM ferrous sulfate plus 0.2% [wt/vol] yeast extract, pH 1.8) at 30°C, as recommended in the DSMZ media guide. Cells that were grown to late stationary phase with regard to ferric ion production were then cycled at least twice, where the culture was permitted to sit overnight with no agitation at 30°C while a portion of the ferric iron in solution was reduced back to the ferrous state. Agitation of the culture resumed in the morning at the rate of 125 rpm in 2-liter flasks with baffles that contained one liter of culture medium, and the subsequent reoxidation of the reduced iron that had accumulated overnight completed the "cycle." Cells treated in this manner were harvested by centrifugation, washed four times with 0.01 N H_2SO_4, and resuspended in sufficient sulfuric acid (pH 1.5) to achieve a stock suspension in excess of 10^{10} cells/ml. Typical yields from 7 liters of culture were 0.18 ± 0.01 g of wet cell paste/l. The stock suspensions were stored at 4°C. Spectroscopic experiments were conducted on aliquots of the cells within the first 3 days following harvesting.

Quantification of bacteria. Absolute numbers of *Fm. acidiphilum* cells were determined by electrical impedance measurements on a Multisizer 4 particle counter (Beckman Coulter, Inc., Brea, CA) fitted with a 30-μm aperture (24, 32). The instrument was programmed to siphon 50 μl of sample that contained

Isoton II as the electrolyte. The current applied across the aperture was 600 μA. Voltage spikes attendant with impedance changes as microorganisms passed through the aperture were monitored with an instrument gain of four.

Relative numbers of *Fm. acidiphilum* cells were determined by photon correlation scattering spectroscopy with a DelsaNano C particle size analyzer, also from Beckman Coulter, Inc. Cell densities were adjusted to $\sim 10^7$ cells/ml in 0.01 N sulfuric acid to produce optimum photon counts in the range of 7,000 to 11,000. Determination of the relative numbers of light scattering particles as a function of particle diameter was accomplished by the time domain method with operating and analysis software provided by Beckman Coulter, Inc.

Total cellular protein was determined using the contents of the Pierce BCA protein assay kit on washed cell pellets after the cells were lysed in a 1% SDS solution as described below for the preparation of samples for the proteomics measurements.

Absorbance measurements with cell suspensions. Absorbance measurements on intact *Fm. acidiphilum* cells in suspension were conducted in an OLIS CLARiTY 1000A spectrophotometer (On Line Instrument Systems, Inc., Bogart, GA) that employed a novel integrating cavity absorption meter (24, 32, 33). In a typical measurement, identical 8-ml solutions that contained sulfuric acid (pH 1.5) were added to both the sample and the reference observation cavities of the spectrophotometer. When the focus of the observation was the production of ferric ions, both the sample and reference cavities initially contained the same concentration of ferrous sulfate. After a stable baseline was recorded from 326 to 476 nm, a small sample was withdrawn from the sample cavity and replaced with an equal volume of suspended *Fm. acidiphilum* to initiate subsequent reactions and absorbance changes within the cavity. When the focus of the observation was the effect(s) of ferrous ions on colored redox-active components within the intact microorganism, both observation cavities initially contained equal suspensions of intact *Fm. acidiphilum*. After a stable baseline was recorded from 417 to 631 nm, a small sample was withdrawn from the sample cavity and replaced with an equal volume of concentrated ferrous sulfate to initiate subsequent reactions and absorbance changes within the cavity. These liquid handling operations were conducted manually. The single opening to the otherwise enclosed observation cavity was subsequently filled with a white, refractive Teflon plug, and data acquisition was then initiated. These latter operations were routinely conducted in 0.5 s, which became the operational dead time for any reaction to proceed before data were obtained.

In either case, raw absorbance spectra, typically 6.2 spectra/s, were then collected for the appropriate time interval. Raw absorbance values obtained in the CLARiTY spectrophotometer were converted to equivalent absorbance values/cm using Fry's method (43) with analysis software provided by OLIS, Inc. Global fits of absorbance changes as a function of both time and wavelength were accomplished by the singular value decomposition method (44) using analysis software also provided by OLIS, Inc. The output of applying the singular value decomposition method is each 3-dimensional data set of absorbances as a function of time and wavelength generated three products as follows: (i) a matrix of spectral eigenvectors that represented the changes in absorbance for the principal absorbing species; (ii) a matrix of kinetic eigenvectors that represented the mechanism that accounted for the time dependences of the principal absorbance change; and (iii) a diagonal matrix of eigenvalues that minimized the differences between the calculated and the observed data.

Genomic sequence similarity searches. tBLASTn sequence similarity searches were conducted on the RefSeq Genome Database maintained for that purpose by the NCBI. The RefSeq assembly accession number for *Fm. acidiphilum* strain T23, DSMZ 19497, was GCA_00949255.1, TaxID number 121039. The query proteins were as follows: CAA29274.1, *Paracoccus denitrificans* aa_3-type; CAC08532.1, *Rhodothermus marinus* caa_3; AAB00370.1, *Thermus thermophilus* ba_3-type; WP_011929405.1, *Vibrio cholerae* 0395 cbb_3-type; A4ZGV2, *Sulfolobus metallicus foxA*-type; P0ABJ9, *Escherichia coli cydA*-cytochrome *bd* subunit 1; and P0ABK2, *E. coli cydB*-cytochrome *bd* subunit 2.

Comprehensive proteomic profiling of *Fm. acidiphilum*. An *Fm. acidiphilum* cell pellet was placed in a 1% SDS solution and immediately homogenized using sonic oscillation. The sample was heated to 80°C for 10 min and the protein concentration was determined using the BCA protein assay kit (Pierce, Thermo Scientific). Based on the protein concentration, 100 μg of protein sample was adjusted to a final volume of 100 μl using 100 mM ammonium bicarbonate; the protein was then reduced using (2-carboxyethyl) phosphine hydrochloride (TCEP) in 10 mm Tris (pH 8.0 at room temperature) at 55°C for 1 h. The reduced sample was subsequently alkylated using 5 μl of 375 mM iodoacetamide at room temperature for 30 min. Next, the protein sample was precipitated by chloroform-methanol extraction, air dried, and digested with 2 μg of trypsin (MS-grade trypsin protease; Thermo Scientific Pierce) at 37°C overnight.

The next day, a SepPak cartridge purification (Waters, Ireland) using acidic reverse phase conditions and an off-line basic reverse phase fractionation step were employed to reduce the complexity of the sample, as previously described (45). Each of the 12 resulting fractions was then run on a Dionex U3000 nano flow high-performance liquid chromatography (HPLC) system coupled to a Thermo Fusion mass spectrometer. Each fraction was subjected to a 90-minute chromatographic method that employed a gradient from 2 to 25% acetonitrile in 0.1% formic acid (ACN/FA) over the course of 60 min, a gradient to 50% ACN/FA for an additional 10 min, a step to 90% ACN/FA for 5 min, and a reequilibration into 2% ACN/FA in a "trap-and-load" configuration. The trap column was an Acclaim C18 PepMap100, 5 μm, 100A and the column was an Acclaim PepMap RSLC 75 μm $\times$ 15 cm (Thermo Fisher Dionex, Sunnyvale, CA). The entire run was conducted at 0.3 μl/min flow rate and the sample was ionized through a Thermo Nanospray Flex ion source. MS1 scans were performed in the Orbitrap utilizing a resolution of 240,000. Data dependent acquisition (DDA) MS2 scans were performed in the Orbitrap using a high energy collision dissociation (HCD) of 30% with a resolution of 30,000. Data analyses were performed using

Proteome Discoverer 2.3 using SEQUEST HT scoring. The protein FASTA database was *Fm. acidiphilum* (TaxID = 1121877) version 2019-12-19. Static modification included carbamidomethyl on cysteines (=57.021), and dynamic modification of oxidation of methionine (=15.9949). Parent ion tolerance was 10 ppm, fragment mass tolerance was 0.02 Da, and the maximum number of missed cleavages was set to 2. Only high scoring peptides were considered, utilizing a false discovery rate (FDR) of 1%.

Data availability. The mass spectrometry proteomics data were deposited to the ProteomeXchange Consortium via the PRIDE (46) partner repository, with the data set identifiers PXD019436 and 10.6019/PXD019436.

SUPPLEMENTAL MATERIAL

Supplemental material is available online only.

SUPPLEMENTAL FILE 1, PDF file, 0.2 MB.

ACKNOWLEDGMENTS

This work was supported by grant numbers 1830866 from the National Science Foundation (R.C.B.) and W911NF-17-1-0518 from the US Department of Defense through its Army Research Office (R.C.B.). The proteomics work was supported by National Institutes of Health grants from the National Center for Research Resources (P20 RR018766-09) (J.J.G.) and the National Institute of General Medical Sciences (P20 GM10351410) (J.J.G.). Funds were also provided by the National Institutes of Health grant P30 GM103514-11 (Phase III) (J.J.G.) and by a special contribution from The Office of the Dean at the Louisiana State University Health Sciences Center (LSUHSC) (J.J.G.).

REFERENCES

1. Johnson DB, Bacelar-Nicolau P, Okibe N, Thomas A, Hallberg KB. 2009. *Ferrimicrobium acidiphilum* gen. nov., sp. nov. and *Ferrithrix thermotolerans* gen. nov., sp. nov.: heterotrophic, iron-oxidizing, extremely acidophilic actinobacteria. Int J Syst Evol Microbiol 59:1082–1089. https://doi.org/10.1099/ijs.0.65409-0.
2. Brierley JA. 1978. Thermophilic iron-oxidizing bacteria found in copper leaching dumps. Appl Environ Microbiol 36:523–525. https://doi.org/10.1128/AEM.36.3.523-525.1978.
3. Norris PR, Owen JP. 1993. Mineral sulphide oxidation by enrichment cultures of novel thermoacidophilic bacteria. FEMS Microbiol Rev 11:51–55. https://doi.org/10.1111/j.1574-6976.1993.tb00266.x.
4. Clark DA, Norris PR. 1996. *Acidimicrobium ferrooxidans* gen. nov., sp. nov.: mixed-culture ferrous iron oxidation with *Sulfobacillus* species. Microbiology 142:785–790. https://doi.org/10.1099/00221287-142-4-785.
5. Jones RM, Johnson DB. 2015. *Acidithrix ferrooxidans* gen. nov., sp. nov.; a filamentous and obligately heterotrophic, acidophilic member of the Actinobacteria that catalyzes dissimilatory oxido-reduction of iron. Res Microbiol 166:111–120. https://doi.org/10.1016/j.resmic.2015.01.003.
6. Norris PR, Davis-Belmar CS, Brown CF, Calvo-Bado LA. 2011. Autotrophic, sulfur-oxidizing actinobacteria in acidic environments. Extremophiles 15:155–163. https://doi.org/10.1007/s00792-011-0358-3.
7. Davis-Belmar CS, Norris PR. 2009. Ferrous iron and pyrite oxidation by "*Acidithiomicrobium*" species. Amr 71–73:271–274. https://doi.org/10.4028/www.scientific.net/AMR.71-73.271.
8. Blake RC, II, Anthony MD, Bates JD, Hudson T, Hunter KM, King BJ, Landry BL, Lewis MS, Painter RG. 2016. *In situ* spectroscopy reveals that microorganisms in different phyla use different electron transfer biomolecules to respire aerobically on soluble iron. Front Microbiol 7:1963. https://doi.org/10.3389/fmicb.2016.01963.
9. Elterman P. 1970. Integrating cavity spectroscopy. Appl Opt 9:2140–2142. https://doi.org/10.1364/AO.9.002140.
10. Fry ES, Kattawar GW, Pope RM. 1992. Integrating cavity absorption meter. Appl Opt 31:2055–2065. https://doi.org/10.1364/AO.31.002055.
11. Hodgkinson J, Masiyano D, Tatam RP. 2009. Using integrating spheres as absorption cells: path-length distribution and application of Beer's law. Appl Opt 48:5748–5758. https://doi.org/10.1364/AO.48.005748.
12. Jávorfi T, Erostyák J, Gál J, Buzády A, Menczel L, Garab G, Razi Naqvi K. 2006. Quantitative spectrophotometry using integrating cavities. J Photochem Photobiol B 82:127–131. https://doi.org/10.1016/j.jphotobiol.2005.10.002.
13. Chance B. 1943. The kinetics of the enzyme-substrate compound of peroxidase. J Biol Chem 151:553–577.
14. Bright HJ, Porter DJT. 1975. Flavoprotein oxidases, p 421–505. *In* Boyer PD (ed), The enzymes XII: oxidation reduction part B, third edition, Academic Press, New York, NY.
15. Lobb RR, Auld DS. 1979. Determination of enzyme mechanisms by radiationless energy transfer kinetics. Proc Natl Acad Sci U S A 76:2684–2688. https://doi.org/10.1073/pnas.76.6.2684.
16. Lobb RR, Auld DS. 1980. Stopped-flow radiationless energy transfer kinetics: direct observation of enzyme-substrate complexes at steady state. Biochemistry 19:5297–5302. https://doi.org/10.1021/bi00564a023.
17. Smith L. 1978. Bacterial cytochromes and their spectral characterization. Methods Enzymol 53:202–212. https://doi.org/10.1016/s0076-6879(78)53025-5.
18. Cox JC, Boxer DH. 1978. The purification and some properties of rusticyanin, a blue copper protein involved in iron(II) oxidation from *Thiobacillus ferrooxidans*. Biochem J 174:497–502. https://doi.org/10.1042/bj1740497.
19. Blake RC, II, Shute EA. 1987. Respiratory enzymes of *Thiobacillus ferrooxidans*: a kinetic study of electron transfer between iron and rusticyanin in sulfate media. J Biol Chem 262:14983–14989.
20. Blake RC, II, Shute EA. 1994. Respiratory enzymes of *Thiobacillus ferrooxidans*: kinetic properties of an acid-stable iron:rusticyanin oxidoreductase. Biochemistry 33:9220–9228. https://doi.org/10.1021/bi00197a025.
21. Yarzabal A, Brasseur G, Ratouchniak J, Lund K, Lemesle-Meunier D, DeMoss JA, Bonnefoy V. 2002. The high-molecular-weight cytochrome *c* Cyc2 of *Acidithiobacillus ferrooxidans* is an outer membrane protein. J Bacteriol 184:313–317. https://doi.org/10.1128/jb.184.1.313-317.2002.
22. Kai M, Yano T, Tamegai H, Fukumori Y, Yamanaka T. 1992. *Thiobacillus ferrooxidans* cytochrome *c* oxidase: purification, and molecular and enzymatic features. J Biochem 112:816–821. https://doi.org/10.1093/oxfordjournals.jbchem.a123982.
23. Sugio T, Ako A, Takeuchi F. 2010. Sulfite oxidation catalyzed by aa_3-type cytochrome *c* oxidase in *Acidithiobacillus ferrooxidans*. Biosci Biotechnol Biochem 74:2242–2247. https://doi.org/10.1271/bbb.100446.
24. Li TF, Painter RG, Ban B, Blake RC, II. 2015. The multi-center aerobic iron respiratory chain of *Acidithiobacillus ferrooxidans* functions as an ensemble with a single macroscopic rate constant. J Biol Chem 290:18293–18303. https://doi.org/10.1074/jbc.M115.657551.
25. Van Gelder BF. 1966. On cytochrome *c* oxidase. I. The extinction coefficients of cytochrome *a* and cytochrome *a3*. Biochim Biophys Acta 118:36–46. https://doi.org/10.1016/S0926-6593(66)80142-X.
26. Kuboyama M, Yong FC, King TE. 1972. Studies on cytochrome oxidase. VIII. Preparation and some properties of cardiac cytochrome oxidase. J Biol Chem 247:6375–6383.
27. Eisen S, Poehlein A, Johnson DB, Daniel R, Schlomann M, Muhling M. 2015. Genome sequence of the acidophilic iron oxidizer *Ferrimicrobium*

acidiphilum strain T23. Genome Announc 3:e00383-15. https://doi.org/10.1128/genomeA.00383-15.
28. Sousa FL, Alves RJ, Pereira-Leal JB, Teixeira M, Pereira MM. 2011. A bioinformatics classifier and database for heme-copper oxygen reductases. PLoS One 6:e19117. https://doi.org/10.1371/journal.pone.0019117.
29. Hemp J, Gennis RB. 2008. Diversity of the heme-copper superfamily in archaea: insights from genomics and structural modeling. Results Probl Cell Differ 45:1–31. https://doi.org/10.1007/400_2007_046.
30. Borisov VB, Gennis RB, Hemp J, Verkhovsky MI. 2011. The cytochrome *bd* respiratory oxygen reductases. Biochim Biophys Acta 1807:1398–1413. https://doi.org/10.1016/j.bbabio.2011.06.016.
31. Giuffre A, Borisov VB, Arese M, Sarti P, Forte E. 2014. Cytochrome *bd* oxidase and bacterial tolerance to oxidative and nitrosative stress. Biochim Biophys Acta 1837:1178–1187. https://doi.org/10.1016/j.bbabio.2014.01.016.
32. Blake RC, II, Griff MN. 2012. *In situ* spectroscopy on intact *Leptospirillum ferrooxidans* reveals that reduced cytochrome 579 is an obligatory intermediate in the aerobic iron respiratory chain. Front Microbiol 3:136. https://doi.org/10.3389/fmicb.2012.00136.
33. Blake RC, II, White RA, III. 2020. *In situ* absorbance measurements: a new means to study respiratory electron transfer in chemolithotrophic microorganisms, p 81–127. *In* Poole R (ed), Advances in microbial physiology, volume 76, 1st edition. Academic Press, New York, NY.
34. Jeans C, Singer SW, Chan CS, VerBerkmoes NC, Shah M, Hettich RL, Banfield JF, Thelen MP. 2008. Cytochrome 572 is a conspicuous membrane protein with iron oxidation activity purified directly from a natural acidophilic microbial community. ISME J 2:542–550. https://doi.org/10.1038/ismej.2008.17.
35. Levican G, Gomez MJ, Chavez R, Orellana O, Moreno-Paz M, Parro V. 2012. Comparative genomic analysis reveals novel facts about *Leptospirillum* species cytochromes. J Mol Microbiol Biotechnol 22:94–104. https://doi.org/10.1159/000338105.
36. Scherrer R, Gerhardt P. 1973. Influence of magnesium ions on porosity of the *Bacillus megaterium* cell wall and membrane. J Bacteriol 114:888–890. https://doi.org/10.1128/JB.114.2.888-890.1973.
37. Plette ACC, van Riemsdijk WH, Benedetti MF, van der Wal A. 1995. pH Dependent charging behavior of isolated cell walls of a Gram-positive soil bacterium. J Colloid Interface Sci 173:354–363. https://doi.org/10.1006/jcis.1995.1335.
38. Brown S, Santa Maria JP, Jr, Walker S. 2013. Wall teichoic acids of Gram-positive bacteria. Annu Rev Microbiol 67:313–336. https://doi.org/10.1146/annurev-micro-092412-155620.
39. Cox JS, Smith DS, Warren LA, Ferris FG. 1999. Characterizing heterogeneous bacterial surface functional groups using discrete affinity spectra for proton binding. Environ Sci Technol 33:4514–4521. https://doi.org/10.1021/es990627l.
40. Ingledew WJ. 1982. *Thiobacillus ferrooxidans*: the bioenergetics of an acidophilic chemolithotroph. Biochim Biophys Acta 683:89–117. https://doi.org/10.1016/0304-4173(82)90007-6.
41. Tuovinen OH, Kelly DP. 1972. Biology of *Thiobacillus ferrooxidans* in relation to the microbiological leaching of sulphide ores. Z Allg Mikrobiol 12:311–346. https://doi.org/10.1002/jobm.19720120406.
42. Ingledew WJ, Cox JC, Halling PJ. 1977. A proposed mechanism for energy conservation during $Fe2^{+}$ oxidation by *Thiobacillus ferrooxidans*: chemiosmotic coupling to net H^{+} influx. FEMS Microbiol Lett 2:193–197. https://doi.org/10.1111/j.1574-6968.1977.tb00938.x.
43. Fry ES, Kattawar GW, Strycker BD, Zhai PW. 2010. Equivalent path lengths in an integrating cavity: comment. Appl Opt 49:575–577. https://doi.org/10.1364/AO.49.000575.
44. DeSa RJ, Matheson IBC. 2004. A practical approach to interpretation of singular value decomposition results. Methods Enzymol 384:1–8. https://doi.org/10.1016/S0076-6879(04)84001-1.
45. Harman JC, Guidry JJ, Gidday JM. 2018. Comprehensive characterization of the adult ND4 Swiss Webster mouse retina: using discovery-based mass spectrometry to decipher the total proteome and phosphoproteome. Mol Vis 24:875–889.
46. Perez-Riverol Y, Csordas A, Bai J, Bernal-Llinares M, Hewapathirana S, Kundu DJ, Inuganti A, Griss J, Mayer G, Eisenacher M, Pérez E, Uszkoreit J, Pfeuffer J, Sachsenberg T, Yilmaz S, Tiwary S, Cox J, Audain E, Walzer M, Jarnuczak AF, Ternent T, Brazma A, Vizcaíno JA. 2019. The PRIDE database and related tools and resources in 2019: improving support for quantification data. Nucleic Acids Res 47:D442–D450. https://doi.org/10.1093/nar/gky1106.